Article:

Al-musawi, H., Figueiredo, F.P., Bernal, S.A. orcid.org/0000-0002-9647-3106 et al. (2 more authors) (2019) Performance of rapid hardening recycled clean steel fibre materials. Construction and Building Materials, 195. pp. 483-496. ISSN 0950-0618

https://doi.org/10.1016/j.conbuildmat.2018.11.026

Performance of rapid hardening recycled clean steel fibre materials

Hajir Al-musawi [a,*], Fabio P. Figueiredo [a], Susan A. Bernal [b], Maurizio Guadagnini [a], Kypros Pilakoutas [a]

[a] *Department of Civil and Structural Engineering, The University of Sheffield, Sir Frederick Mappin Building, Mappin Street, S1 3JD Sheffield, UK.*

[b] *School of Civil Engineering, University of Leeds, Woodhouse Lane, Leeds, LS2 9JT, United Kingdom.*

* Corresponding author's email: Haal-musawi1@sheffield.ac.uk Tel: +44 (0) 114 222 5729, Fax: +44 (0) 114 2225700

HIGHLIGHTS

- Mixes achieve 90% of their one year flexural strength at the age of one day.
- RCSF enhances flexural strength and toughness resulting in hardening behaviour.
- Constitutive equations based on the RILEM and MC 2010 recommendations overestimate loading capacity.
- FEA analysis using multilinear σ – ε tensile curves obtained by inverse analysis can capture well the post cracking strength and cracking pattern.

Abstract

To minimise disruption due to repairs of concrete pavements, rapid hardening and tough materials need to be used. This paper investigates the flexural performance of rapid hardening mortar mixes made with two commercial cement types, calcium sulfo-aluminate cement and calcium aluminate cement, for thin concrete repair applications. Three-point bending tests are performed on plain and steel fibre reinforced

concrete specimens containing 45 kg/m^3 of recycled clean steel fibres to characterise the flexural performance of notched and unnotched prisms at different ages, ranging from one hour up to one year. The recycled fibers are shown to enhance both the flexural strength and toughness of FRC prisms, leading to hardening behaviour. Constitutive equations based on the RILEM and Model Code 2010 recommendations are found to overestimate the loading capacity of the bending tests. FE analyses using multilinear $\sigma - \varepsilon$ tensile curves obtained by employing inverse analysis can capture better the post cracking strength and cracking pattern of the tested prisms.

Key words*:* SFRC, recycled clean steel fibres, rapid hardening cements, mechanical properties, FEA

1. Introduction

Progressive deterioration of infrastructure, particularly pavements, occurs due to increasing vehicular axle loads, worsening environmental conditions (due to climate change) and higher traffic volumes. Excessive deterioration can lead to serious service disruptions and higher costs for infrastructure owners and road users. Conventional ordinary Portland cement (OPC) based repair materials attain their strength rather slowly and need between 12h to 24h to develop sufficient strength before roads can be back in service, adding to delays and disruption during maintenance. To minimise disruption, rapid hardening cements can be used in repairs. There are several special rapid hardening Portland-free cements available in the market; such as calcium sulfo-aluminate (CSA) cement and calcium aluminate (CA) cement. CSA can achieve early rapid strength development even in cold environments and can have expansive properties. It is reported to have good durability in aggressive environments, particularly when exposed to sulfates [2]. Furthermore, this cement requires less energy for its production compared to OPC [1], thus it is considered to be environmentally friendly. However, despite its lower energy demand, it is still more expensive due to the cost of its raw materials.

CA cements are characterised by high early strength development and high resistance to elevated temperatures, depending on their aluminum content. An important aspect for the rapid strength development of this cement is the substantial amount of heat of hydration which can result in high heat generation [3]. Self-heating may be a concern in sections thicker than 100 mm [3], but not necessarily for thinner repair layers. Despite the high temperature rise during hydration, CA concretes do not seem to be overly susceptible to thermal cracking. This may be due to creep relaxation of thermally induced strains, facilitated by a conversion reaction, during which some metastable phases of this cement convert to stable phases of lower volume [3, 4]. As porosity increases, the densification due to conversion causes loss of strength [3]. Hence, when used for repairs, the key concern to be addressed is cracking due to restrained shrinkage.

Restrained shrinkage is one of the main factors that govern the serviceability and durability of concrete repairs [5,6]. Shrinkage in concrete results due to moisture diffusion from the new concrete to the environment and to the concrete substrate [7] if not adequately saturated. However, shrinkage deformation (of the new layer) is restrained by the substrate layer leading to the development of tensile and interfacial shear stresses. If these stresses exceed the material capacity at any time, cracking will develop in the repair material and/or debonding along the interface between the repair material and the substrate. Micro-cracks induced by shrinkage can propagate and coalesce into macro-cracks under the effect of applied loads.

Cracks beyond a certain width can adversely affect the durability of repair materials by creating easy access for deleterious agents leading to early saturation, freeze–thaw damage, scaling, and steel corrosion, which promote further internal and external cracking and accelerate the rate of deterioration [8]. This issue can be worsen with rapid hardening (non-expansive) materials due to the rapid hydration rate which accelerates shrinkage development. Furthermore, due to the rapid stiffness development and decrease in creep compliance of rapid hardening cements [9], their ability to redistribute stresses may be affected, thereby increasing cracking potential. To address this issue, fibres can be added to control crack widths [10] as well as increase the tensile strength and fatigue resistance [11], thus resulting in more durable layers. To reduce the environmental impact of manufactured steel fibres (MSF), recycled clean steel fibres (RCSF) can be used as alternative fibre reinforcement.

During the manufacture of tyres, parallel steel cords are embedded in continuous thin rubber belts. After being cut to shape, these are placed in overlapping layers to provide flexible reinforcement within the tread and side walls of the tyre. The complex configuration of each layer generates significant levels of waste (approximately 5% by mass). The available amount of waste steel cord is therefore around 100,000 tonnes per year worldwide. The steel reinforcement used in tyre manufacture typically consists of parallel filaments of very fine wire (0.1-0.4 mm dia.) twisted together to form a cord about 0.5-1.0 mm in diameter [12]. Recycled clean steel fibre (RCSF) filaments extracted from pre-vulcanised rubber belt offcuts have become available recently and were adopted in this study. However, knowledge on their use in concrete is scarce and it is limited to research at the University of Sheffield [13]. Knowledge of the effect of industrial fibres on CSA and CA matrices is also rather limited [9,14-16] and no published data exist regarding the effect of RCSF. A study on the effect of CSA matrix on pullout performance of steel fibres [9] suggests that the synergetic effect of a stiff matrix like ettringite and high modulus steel fibres can increase crack propagation in the composite material, evidenced by an increase in debonding energy density.

Since cracking is the main concern for repairs, understanding the effect of fibres in controlling crack widths under mechanical and hygral loads, as well as the complex interaction of shrinkage, stiffness and tensile strength evolution are of paramount importance. For this purpose, finite element analysis can be a useful tool. However, appropriate material parameters need to be determined experimentally and the tensile σ-ε curves of the repair materials need to be derived from direct tension or bending results. Although there are several procedures in the literature to derive the σ-ε of SFRC in tension [17-20], they may not be entirely suitable for modelling mortars reinforced with RCSF due to the different fracture energies of the two concretes. In numerical studies performed by [20, 21], it was found that RILEM proposed σ-ε equations overestimate the predicted capacity of FRC. As a result, a simplified σ-ε model was suggested to overcome issues in the other methods and to include the post-consumer tyres steel fibres (RTSF) effect.

This paper presents experimental and numerical work on the flexural performance of RCSF on rapid hardening mortars produced using CSA or CA as sole cementitious materials. Constitutive relationships derived based on code recommendations and by others [19, 20] are used to predict flexural behaviour and the results are compared with predictions obtained from inverse analysis.

2. Experimental details and methodology

2.1. Materials

Two commercial cement types were used in this study; calcium sulfoaluminate cement[1] (CSA) and rapid setting calcium aluminate cement[2] (RSC). According to the manufacturer, RSC consists of hydrated alumina, oxides of iron and titanium, with small amounts of silica. For production of mortars, fine aggregates, medium grade river washed sand (0-5mm sourced from Shardlow in Derbyshire, UK, SG=2.65, A = 0.5, FM = 2.64), were used. Recycled clean steel fibres (RCSF) were obtained from tyre cords extracted from un-vulcanised rubber belts (see Figure 1). The length of the RSCF used in this study was 21 mm and the diameter 0.2 mm. The strength of these fibres is reported to exceed 2600 MPa [13]. Superplasticiser[3] was added to enhance the workability and adjust the setting time.

Figure 1. Photograph of the RCSF used in this study

2.2. Mortar mix design

A total of 600 kg/m^3 of cement was used with low w/c ratios to obtain high early strength. For durability requirements, w/c should be kept lower than 0.4. However, as CSA cement consumes more water to form hydration products than ordinary Portland cement [22], this limit can be relaxed slightly for this cement. As a result, two different w/c ratios and SP dosages were tested. The w/c ratios for mixes with CSA cement were 0.4 and 0.41, and 0.35 and 0.36 for RSC mixes. The water content and superplasticiser (SP) were carefully selected to achieve a workable mix with setting time of no longer than 15 minutes. Fibre dosage of 45 kg/m^3 (V_f = 0.57%) was investigated as is commonly used in European practice for structural applications. The plain and fibre reinforced mortar mixes for each cement type are almost identical, to reliably investigate the effect of fibres on the mechanical properties. The details of the optimised mortar mixes are summarised in Table 1.

The specimens were cured for one hour before demoulding and exposure to standard laboratory conditions.

Table 1

---

[1] provided by Kershin International Co., Ltd
[2] sourced from Instarmac
[3] Sika Viscoflow 2000

Mortar mix composition

mix	Cement (kg/m^3)	w/c	Sand (kg/m^3)	SP[a]	Fibre dosage (kg/m^3)
CSA	600	0.40	1420	0.60	0
FCSA	600	0.41	1420	0.61	45
RSC[b]	600	0.35	1300	0.20	0
FRSC	600	0.36	1300	0.21	45

[a] % by cement mass. [b] mixes containing CA cement are called RSC in this study.

2.3. Fresh state properties

2.3.1. Vicat test

The setting time of cement pastes was assessed using an automatic Vicat apparatus according to ASTM C191 (2013) [23]. As the cements used in this study are fast setting, the instrument was set to take measurements every 30 seconds.

2.3.2. Semi-adiabatic calorimetry

The semi-adiabatic calorimeter records the temperature evolution and key temperature related properties for a tested mix, such as time to peak heat, peak heat, and cumulative heat [24]. Since the mortar mixes are designed for thin repairs, heat loss due to dissipation is expected to take place and hence, the semi-adiabatic test could reveal a temperature evolution that is close to practical applications. After mixing the required quantity for each mix, the mortar was directly placed in an insulated thermal flask cylinder of 0.5 l and a thermocouple was inserted inside the mortar to record the temperature.

2.4. Flexural tests

To characterise the flexural performance, mortar prisms of 40 × 40 × 160 mm were tested according to BS EN 13892-2 [25]. To obtain the load deflection curve after the peak load, displacement control was adopted rather than load control as required by the standard. The rate of loading was 0.25 mm/min until 1 mm deflection, and 1 mm/min after that. To eliminate errors due to machine stiffness, spurious support displacements and local concrete crushing, a specially designed aluminum yoke (based on the Japanese standard JSCE-SF4 [26]) was mounted on the specimens. To assess the flexural behaviour over time, the prisms were tested at one hour, three hours, one day, seven days, 28 days and 365 days. The test was also performed on notched prisms (the notch depths range from 3.57 to 4.94 mm) to assess crack development. The Crack Mouth Opening Displacement (CMOD) was measured at mid span with a 12.5 mm clip gauge (mounted across the bottom part of the notch, Figure 2). For practical reasons, this test was performed at 2 days (at the earliest age) and up to one year.

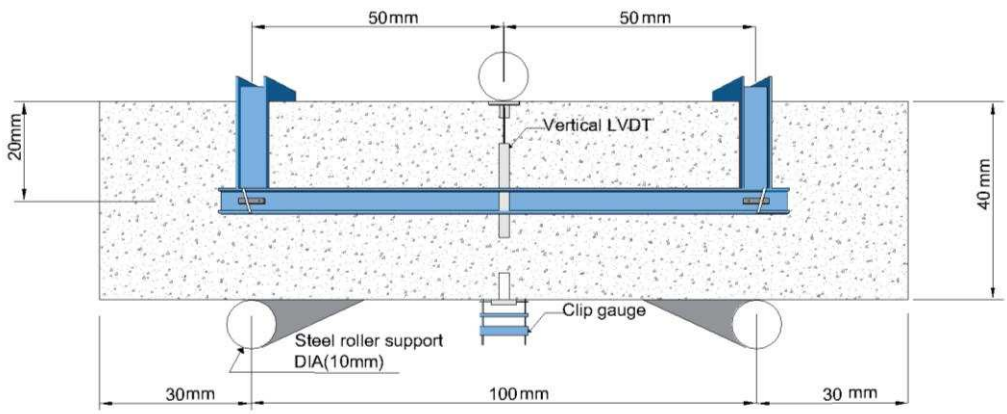

Figure 2. Flexural test set up

2.5. Compressive strength

Directly after flexural testing, the halves of the fractured prisms were tested in uniaxial compression according to BS EN 13892-2 [25]. Only the one-hour compressive strength of FRC specimens was examined separately due to practical time constrains.

3. Experimental Results and Discussion

3.1. Fresh state properties of rapid hardening materials

The water content and SP dosage were optimised for each mix to achieve a workable mix with setting time of no longer than 15 minutes. As shown in Table 2, the CSA cement had a relatively shorter setting time compared to the RSC cement. Slightly higher water content and SP dosages for the fibre reinforced mixes lead to a slight increase of the setting time for these mixes.

Table 2

Setting time and maximum temperature (T_{peak}) for different mixes

Mixes	Vicat setting time (min.) Initial	Final	T_{peak} (°C)
CSA	9.5	10.5	68
FCSA	9.5	11.0	68
RSC	12.0	14.5	91
FRSC	12.5	15.0	88

The results of the semi-adiabatic calorimetry test (for the first 36 hours) are shown in Figure 3. For mixes with CSA cement, the peak temperature (T_{peak}) was about 68° C (see Table 2) occurring during the first hour regardless of fibre content. The temperature rise in RSC mixes was much higher than in mixes with CSA cement, with T_{peak} at 91° and 88° C for RSC and FRSC, respectively. The time half way to the peak ($T_{1/2\ peak}$) can be taken as an indication of the initial setting time of cementitious mixes [27]. For CSA and FCSA, $T_{1/2\ peak}$ was achieved at around 11 minutes, whilst for RSC and FRSC, it was recorded at around 16 minutes. These results agree well with the results of the vicat test. The temperature achieved for these cements upon hydration dropped to laboratory temperature in less than 24 hours. Heat dissipation is expected to occur faster onsite than in the semi-adiabatic test and, therefore, no major thermal cracking is expected for thin repairs, especially when curing is applied during the first two hours when T_{peak} occurs.

3.2. Mechanical performance of rapid hardening mortars

3.2.1. Compressive strength

The average compressive strength f_{cu} (from six specimens) and standard deviation developed over time is shown in Figure 4. At one hour, FCSA achieved the highest compressive strength of 26.1 MPa while RSC achieved 17.2 MPa. This behavior changes at later ages as RSC achieves a higher strength than FCSA by approximately 6% after one-year. The fibres seem to have a positive effect on the compressive strength of both mortars, with the highest strength increase noticed at one hour (24% increase in f_{cu}). At later ages, this increase ranges from 10% to 17%.

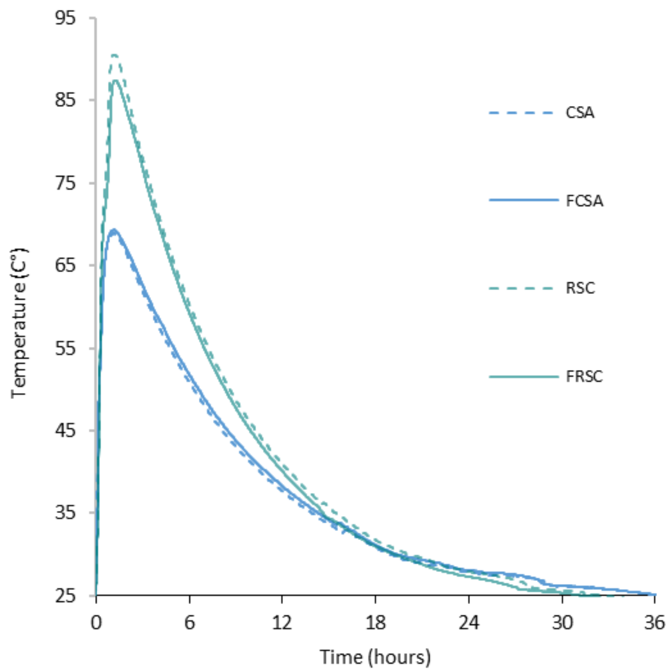

Figure 3. Temperature rise for mixes in semi-adiabatic test

There is no consensus in literature on the effect of fibers on compressive strength. While some researchers [28-30] report a strength enhancement of up to 20% for Portland cement-based specimens containing recycled fibres with dosages less than 50 kg/m^3, others [31-33] found only a marginal effect due to air entrainment.

No strength reduction has been observed for any of the mixes at the age of one-year, indicating that there were no significant conversion issues. It should be noted that for fully cured rapid hardening CSA mortar-based samples (tested at 28 days), a compressive strength of 31.4 – 52.6 MPa for w/c ratios 0.4

– 0.5 was reported in literature [34] and this agrees well with the results of this study.

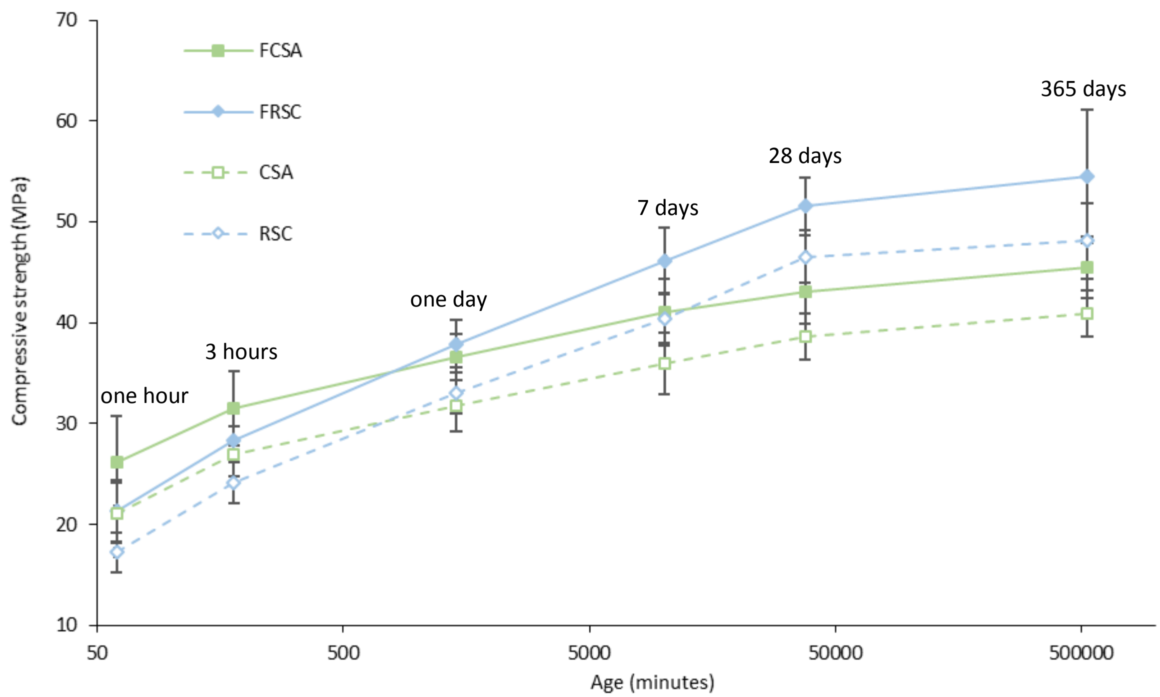

Figure 4. Development of f_{cu} as a function of time

To describe the compressive strength development with time, the $\beta_{cc}(t)$ function that describes the strength development with time used in Model Code 2010 [18] is followed.

$$\beta_{cc} = \exp\{s.[1 - (\frac{28}{t})^{0.5}]\} \qquad equation\ 1$$

where, t is the concrete age in days, s is a coefficient that depends on the class of cement which ranges from 0.2 – 0.38 for $f_{cm} \leq 60$ MPa. As the cements used in this study are rapid hardening, a 0.2 value for s was adopted. To obtain the strength at various ages, $\beta_{cc}(t)$ is multiplied by the mean compressive strength at the age of 28 days (f_{cm}). The estimated compressive strength at various ages is shown against the experimental results in Figure 5. As expected, the function underestimates the strength at the early ages by approximately 100% for the different rapid hardening mixes. As the strength evolves very rapidly at the early ages and then it slows down, smaller s values could offer a better representation for strength development with time. The s values of 0.024 and 0.044 for mixes with CSA and RSC cements, respectively, were found by regression analysis to represent well the strength evolution with time (see Figure 5).

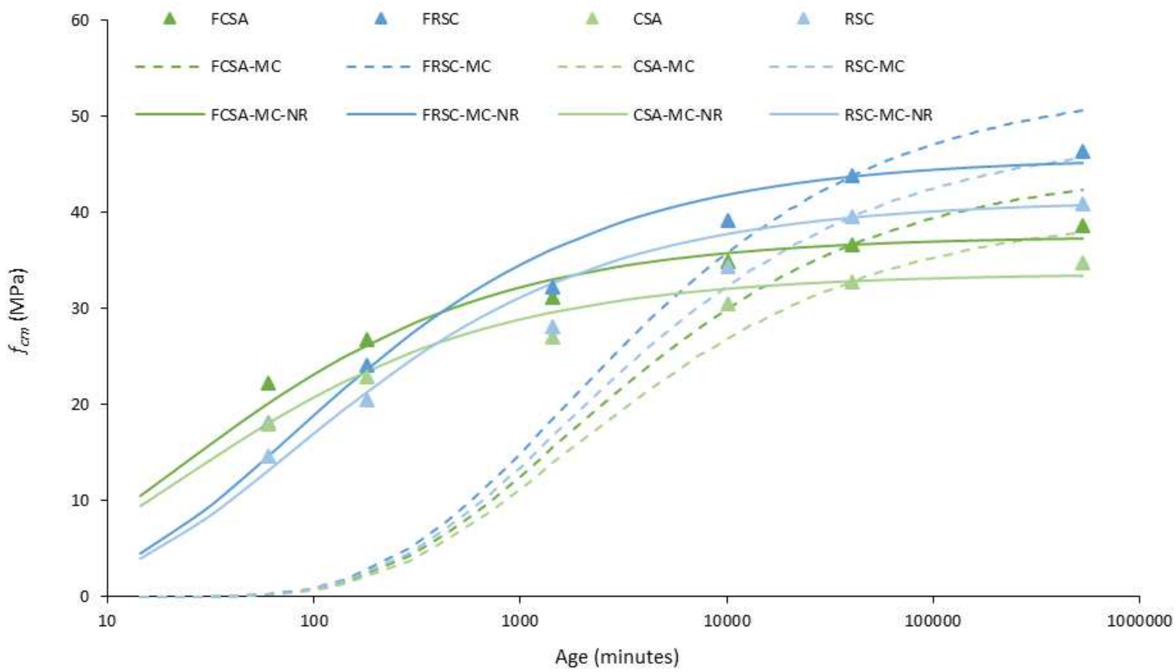

Figure 5. Development of experimental and estimated f_{cm} as a function of time using s = 0.2 (dashed lines) and suggested s values (solid lines-NR)

3.2.2. Flexural behaviour

The average flexural strength development over time (and standard deviation) is illustrated in Figure 6. The reported values represent the limit of proportionality (LOP), or first cracking strength ($f_{\mathrm{ctm},fl}$), determined according to BS EN 14651:2005 [35]. It is noted that strength develops very fast and both plain and fibre reinforced specimens achieved 90% of their one-year strength in one day. The specimens made with CSA cement showed higher flexural strength than those with CA cement tested at the same age, probably due to the rigid dense crystal microstructure of the CSA cement [9]. RSC mixes have lower w/c ratio, hence, their compressive strength is expected to be higher in the long term. Due to high shrinkage in RSC mixes, their flexural strength is reduced. The effect of RCSF on the flexural strength enhancement of the mixes is evident at all ages. Compared to their plain counterparts, FCSA and FRSC mixes showed a flexural strength increase of approximately 36% to 70% and 24% to 41%, respectively. This agrees well with Hu et al. [33], who reported an increase of 45% - 70% in $f_{ctm,fl}$ of concrete reinforced with blends of manufactured and post-consumer recycled fibres.

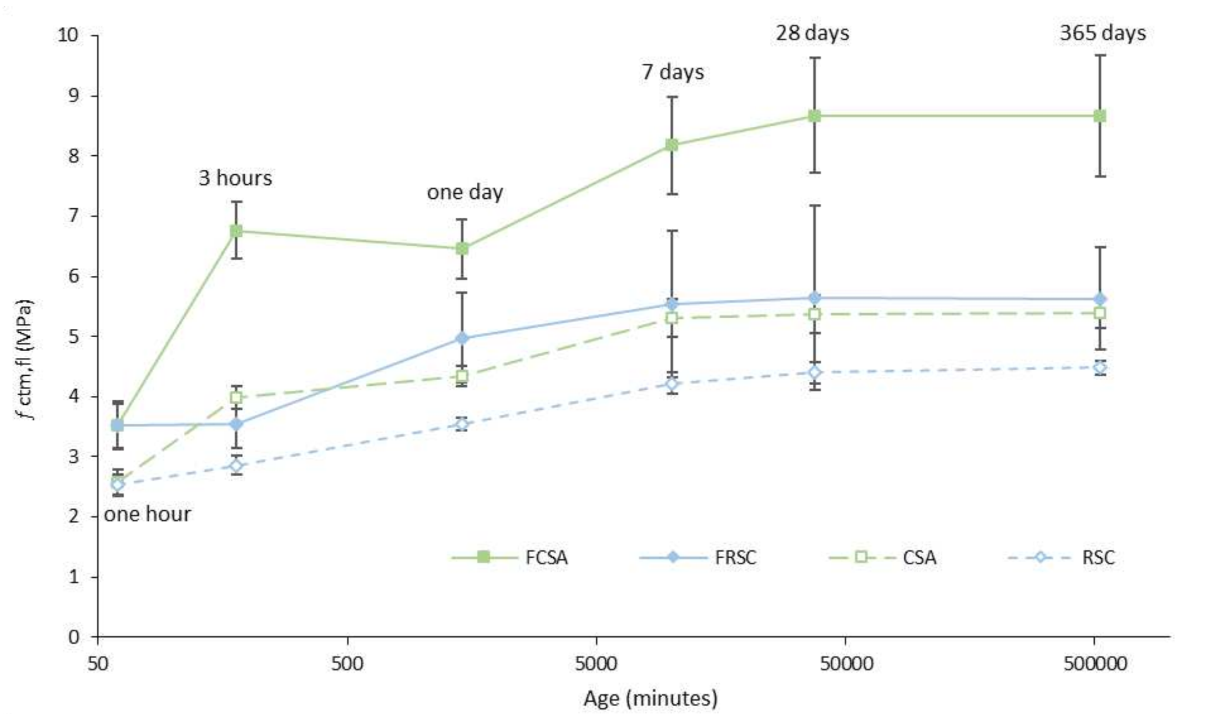

Figure 6. The flexural strength $f_{ctm,fl}$ development as a function of time

The load-deflection curves for FCSA and FRSC prisms are shown in Figure 7. The behaviour of the specimens made with the unreinforced mixes is not shown as they failed suddenly after peak load without any post cracking strength, highlighting the poor toughness of plain mortars in tension. The deflection hardening shown by reinforced mixes can be attributed to the high number of fibres spanning the cracked section and the excellent bond between steel fibres and dense matrix systems, like the CSA cement. This hypothesis is supported by the fact that in the current study, many specimens developed more than one principal crack, confirming the excellent load transfer by the RCSF. It should be noted that the preferential alignment of the fibres in the direction of stress due to the small mould size (40 ×

40 × 160 mm) may have contributed to this. Deflection hardening was also reported in a study by Bordelon [36] for concrete specimens cut from prisms of 150 × 150 × 450 mm and tested using a 50 mm beam depth (to simulate a thin overlay). Deflection hardening performance for notched concrete prisms reinforced with 45kg/m^3 of blends of recycled post-consumer and manufactured steel fibres was also reported in a recent study published by Hu et al. [33].

At large deflections (greater than 2 mm), the FCSA specimens show a slight reduction in load resistance compared to FRSC specimens, possibly due to the inherent brittleness of the CSA cement. However, in most repair applications, it is not expected that the mortar will reach such high level of deformation and as a result, minimal cracking is expected.

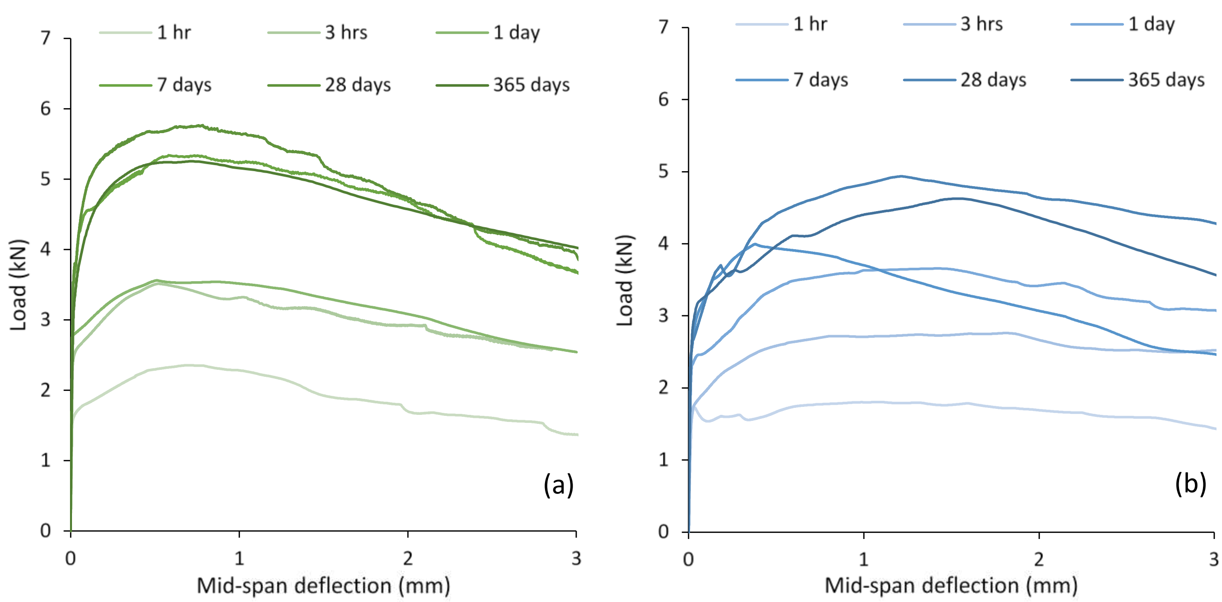

Figure 7. Load-deflection response of rapid hardening fibre reinforced mortars tested at different ages: (a) FCSA; (b) FRSC

3.2.3. Flexural modulus of elasticity (E_{fm})

The flexural modulus of elasticity (E_{fm}) was determined from load-deflection curves using elastic analysis and ignoring shear deformations. E_{fm} is the maximum flexural modulus between 30 – 60% of the peak load (P_{peak}) [37]. Figure 8 shows the development of E_{fm} and related standard deviations over time for all mixes. The plain mortar mixes are shown in dotted lines. As with flexural strength, the stiffness of the mixes develops quickly and reaches around 90% of the one year modulus within 7 days.

The fibres have a remarkable effect on the modulus of elasticity. FCSA and FRSC have higher E_{fm} compared to CSA and RSC mixes respectively with the highest noticeable increase (29.7%) for FCSA occurring at one-hour of age. This behaviour was not reported in [33] and [38] who only noticed a marginal effect on the modulus of concrete with fibre addition. The remarkable increase in modulus of elasticity, though also reflected in the flexural strength, is beyond what is expected from a perfect composite. This may be partially due to fibre alignment, but also to the slightly longer mixing time that was necessary to integrate the fibres. An increase of approximately 36% in the modulus of elasticity of OPC based mortars reinforced with 2% (by volume) industrial steel fibres was reported in literature [39].

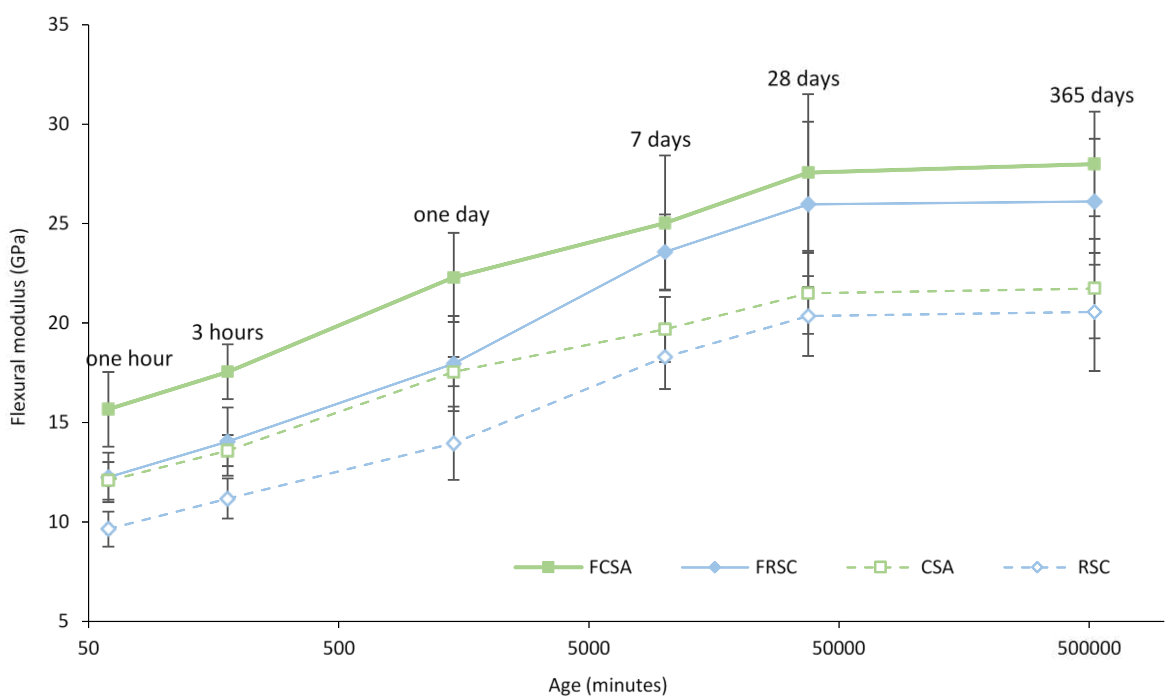

Figure 8. Flexural modulus (E_{fm}) of fast setting fibre reinforced mortars as a function of time

To estimate the modulus of elasticity of the mixes, based on compressive strength, equations from Model code [17], ACI 318-05 [40] and Kosaka et al. [41] were used. The latter equation was developed specifically for mortars. The estimated modulus of elasticity (E_c) for CSA (using the above equations) is presented in Figure 9. As shown, the equations overestimate E_c for CSA mix, especially at the early ages. It should be noted that both Model code and ACI code adopt equations that use the 1/3 and 1/2 power of f_{cm} respectively. However, the results show that for these mortars, the linear relationship is more appropriate and the constant values of 720, 580, 640 and 520 were determined by regression analysis for FCSA, FRSC, CSA and RSC mixes respectively.

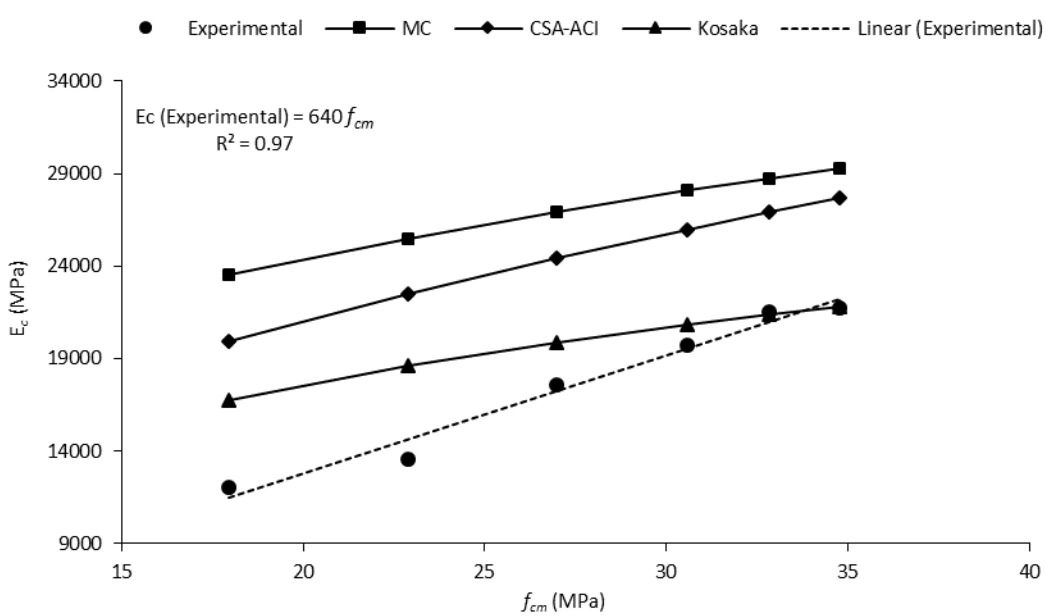

Figure 9. The relationship between f_{cm} and E_c using different equations for CSA mix

3.2.4. Relationship between measured deflection and CMOD values

A linear relationship between CMOD and average deflection is suggested in BS EN 14651:2005 [35], as given below,

Average deflection (mm) = k × CMOD (mm) + 0.04 mm, k = 0.85

This linearity has also been confirmed for FCSA and FRSC at all ages tested with coefficients of determination $R^2 > 0.99$, but as expected with lower K values, between 0.55 and 0.65, due to the different geometry of the testing arrangement. It should be noted that the CMOD measured by the clip gauge is corrected for the position of the clip gauge using the BS EN 14651:2005 [35].

A relationship between deflection and CMOD can facilitate the testing of such materials by using clip gauges only to measure the CMOD as accurate measurement of deflection requires the use of a special frame (yoke) to obtain net deflection. It also provides a benchmark for comparisons.

3.2.5. Residual flexural tensile strength (f_R)

RILEM TC 162-TDF [42] presents a methodology to calculate the residual flexural tensile strength of SFRC prisms, which was later adopted by BS EN 14651:2005 [33]. Residual flexural stresses (f_{R1}, f_{R2}, f_{R3} and f_{R4}) are calculated from the load-CMOD curves at 0.5, 1.5, 2.5 and 3.5 mm of CMOD, respectively. However, these CMODs are suggested for concrete prisms of 500 mm span length. For this study, the residual stresses are calculated at CMOD equal to 1/5 of those used for 500 mm span specimens; i.e. 0.1, 0.3, 0.5 and 0.7.

Figure 10 shows the f_{Ri} values of all FCSA and FRSC mixes tested at different ages. The f_R values for FCSAs are shown in solid lines while FRSCs are shown in dashed lines. It is noticed that for both mixes the f_R values continue to increase from CMOD 0.1 mm to 0.7 mm which shows the high efficiency of the RCSF in carrying the loads across cracks. This is also evidenced by the multiple cracks that form in some samples at, or more than, seven days of age. The residual strengths of FCSA are higher than those of FRSC for the same crack width, which implies better bond strength for RCSF in FCSA matrices.

The f_R values continue to increase with time for both FRC mixes and reach their peak values at 28 days. However, there is a slight strength reduction at one year compared to 28 days. This could be attributed to the effect of the conversion reaction occurring in the RSC cement. This is unlikely, however, as there was no reduction in compression strength at one-year of age. Another possible explanation is the effect of shrinkage on the bond strength of RCSF. This reduction in f_R is more obvious at higher CMOD levels (for f_{R2} to f_{R4}), which means that the frictional resistance along the fibres reduces slightly at one year.

Figure 11 and Figure 12 show the relationship of f_{R1} vs f_{R2}, f_{R1} vs f_{R3} and f_{R1} vs f_{R4} for FCSA and FRSC, respectively. The values of f_{R2}, f_{R3} and f_{R4} correlate very well with f_{R1} for FCSA prisms with $R^2 \geq 0.98$. A similar trend was also found for FRSC prisms, however, with a relatively smaller coefficient of determination ($R^2 \geq 0.92$). A linear relationship between f_{R1} vs f_{R3}, f_{R1} vs f_{R4} were also reported by Zamanzadeh et al. [43] for unclassified RTSF. The strong correlation between the f_R values can lead to simpler design guidelines.

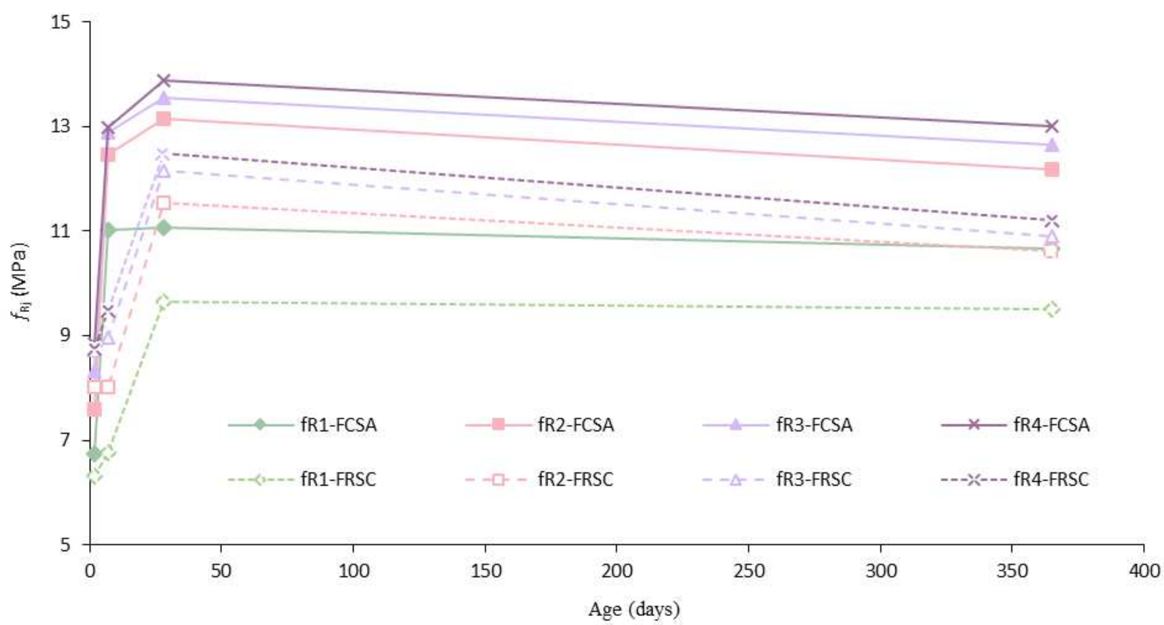

Figure 10. f_R values of FCSA and FRSC prisms (in MPa) development with age

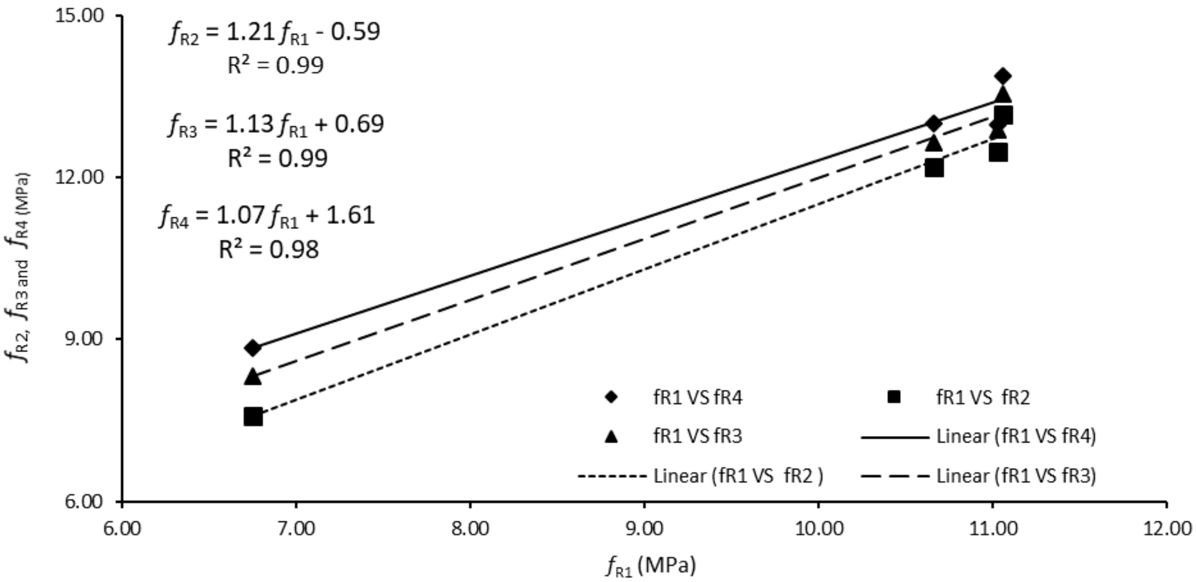

Figure 11. Correlation between f_{R1} and f_{R2}, f_{R1} and f_{R3}, f_{R1} and f_{R4} of FCSA prisms

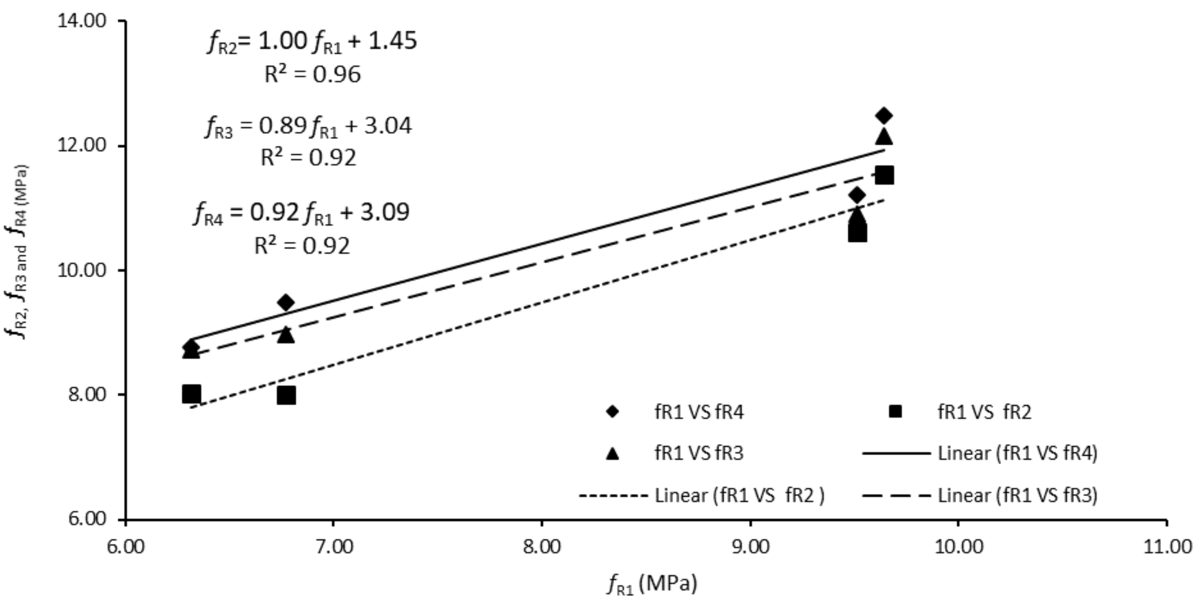

Figure 12. Correlation between f_{R1} and f_{R2}, f_{R1} and f_{R3}, f_{R1} and f_{R4} of FRSC prisms

4. Numerical study

4.1. FE modelling

To model the flexural performance of these materials, the FE package ABAQUS is used, which offers three material models for concrete simulation; Concrete Smeared Cracking (CSC), Brittle Cracking (BC) and Concrete Damaged Plasticity (CDP) [44]. It was found that, for this application, CSC is prone to numerical instabilities soon after crack development. Similar issues were also reported in [45] when modelling SFRC prisms using CSC. Although the BC model was applied successfully to model FRSC [46], it was considered unsuitable for the current study as it assumes that the concrete remains elastic in compression. Since, due to the high flexural strength of the mortars, in this study, the material is expected to become non-linear in compression. Therefore, the analysis was performed by using the concrete damage plasticity (CDP) model for which the user can define the tensile and compression behavior of concrete in as many steps as required. In CDP, the ratio of biaxial to uniaxial compressive strength (σ_{b0}/σ_{c0}) and the ratio of the second stress invariant on tensile meridian to that on the compressive meridian (K_c) characterise the failure surface of concrete. The dilation angle (ψ) and flow potential eccentricity (ε) are used to define the flow rule [44]. σ_{b0}/σ_{c0} was taken as 1.2 (slightly higher than the value usually assigned for plain concrete due to presence of fibres), K_c was 0.667, ψ was 31° and after a sensitivity analysis for ε, the default value of 0.1 was adopted. The CDP model can be regularised by using viscoplasticity to assist in overcoming convergence issues, that occur in materials exhibiting softening behaviour in implicit analysis computations, by permitting the stress to be outside the yield surface. Since high values of viscosity (μ) compared to characteristic time increment can compromise the results, a value of zero was adopted.

Unnotched beams under 3-point bending were modelled in Abaqus with the same dimensions as tested. The mesh was kept constant at 10 mm size (Figure 13) and a 3D 20-noded quadratic brick element with reduced integration (C3D20R) was chosen, as second-order elements are very effective in bending-dominated problems [44]. Uniform displacement control loading was applied to minimise convergence problems and to better simulate the experimental loading conditions.

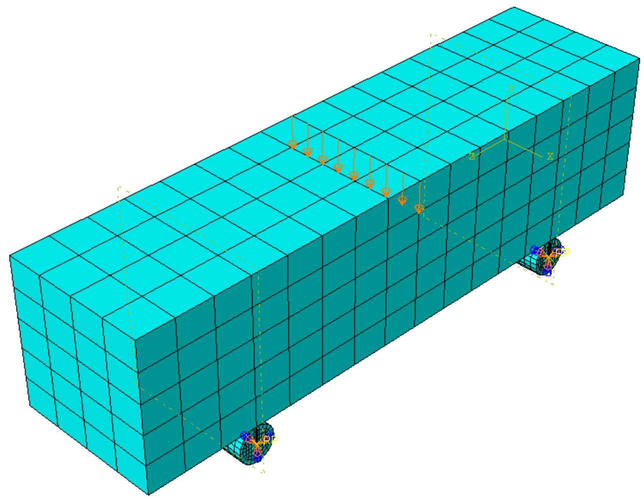

Figure 13. Prism assembly in Abaqus

4.2. Evaluation of tensile constitutive equations

RILEM TC 162-TDF (RILEM) [17], MODEL CODE 2010 (MC) [18], Barros et al. (Barros) [19] and Hu et al. (Hu) [20] procedures were selected to derive the tensile constitutive equations. Although MC allows the use of stress-crack width relationship, RILEM, Barros and Hu models all use stress-strain relationships, and since stress-crack width relationship also leads to mesh dependency in CDP, it was decided to the use stress-strain approach in modelling, to be able to make a direct comparison between different models. The derived tensile σ-ε relationships (see Table 3) using the aforementioned procedures were implemented in Abaqus to determine the load-deflection response of FCSA and FRSC prisms (at 28 days). MC requires the maximum value of crack width (w_u) to calculate the stress at ultimate strain. The value 0.5 mm was used for the max crack width as it corresponds to $CMOD_3$.

The predicted numerical load-deflection curves are compared against the experimental results for FCSA in Figure 14. It can be seen that all the approaches fail to model the full behaviour of the prisms and for most of them the analysis does not converge beyond 0.6 mm (even after using high values of μ). At 0.2 mm deflection, RILEM, MC and Barros overestimate the loading capacity by 29.44%, 16.65% and 7.11% while Hu underestimates the loading by 14.88% respectively. Barros's model, however, can capture the post-cracking behaviour of FCSA up to a certain extent. The models are even less effective in predicting the flexural behaviour of FRSC (see Figure 14). Overall, none of the above models seem to be able to capture the complete load-deflection behaviour of the tested specimens.

Table 3

σ-ε relationships for FCSA and FRSC at 28 days using different approaches

Mixes	RILEM		MC		Barros		Hu	
	σ	ε	σ	ε	σ	ε	σ	ε
FCSA	9.473	0	2.980	0	7.037	0	4.771	0
	4.977	0.000263	3.311	0.000030	3.981	0.001056	2.986	0.001892
	5.140	0.024814	4.977	0.002319	3.751	0.103864	3.929	0.024857
	0.095	0.025000	4.561	0.012335	0.080	0.104000	0.050	0.025000
	0.090	0.500000	0.030	0.012500	0.074	0.500000	0.048	0.500000
			0.029	0.500000				
FRSC	6.165	0	3.354	0	4.580	0	3.105	0
	4.340	0.00017	3.727	0.000006	3.472	0.001066	2.604	0.002019
	4.619	0.024822	4.340	0.002333	3.370	0.103870	3.523	0.024864
	0.070	0.025000	4.145	0.012340	0.050	0.104000	0.040	0.025000
	0.065	0.500000	0.040	0.012600	0.046	0.500000	0.035	0.500000
			0.035	0.500000				

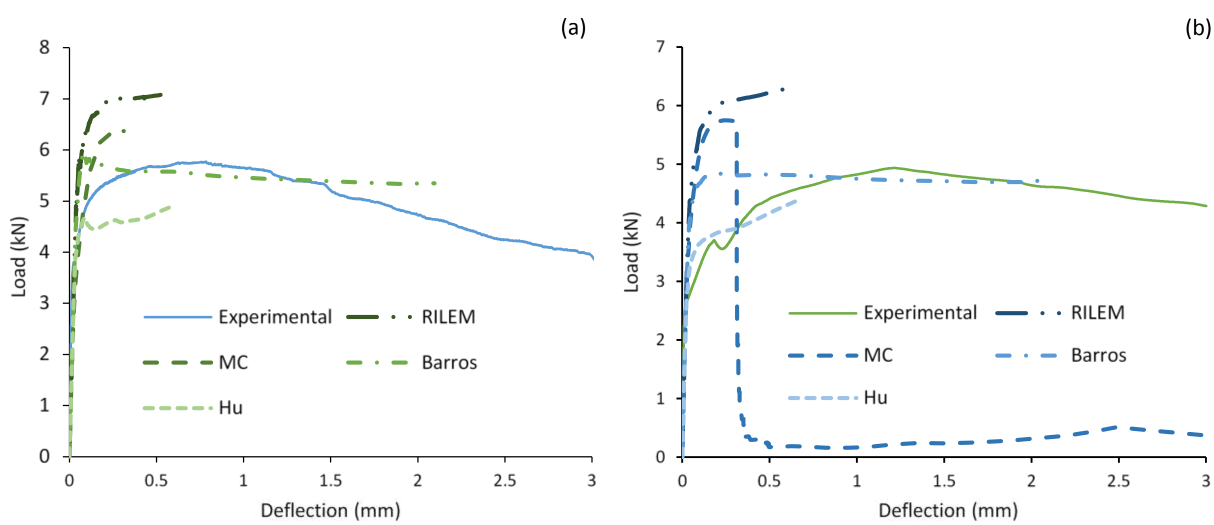

Figure 14. Comparison between experimental and numerical load-deflection curves at 28 days for: (a) FCSA; (b) FRSC

4.3. Numerical approach using inverse analysis

Inverse analysis was adopted to determine the post-cracking σ – ε relationships for the different SFRC mixes and obtain a better prediction of the flexural performance of the tested specimens. The tensile properties are defined by using multilinear σ – ε curves. The analysis is repeated while adjusting the tensile parameters until the numerical load-deflection curve matches the experimental response in capacity and energy dissipation within 2%.

The determined tensile σ – ε curves shown in Figure 15 are then used to predict the structural behaviour of the FRC tested specimens. To better capture the flexural performance at larger displacements, the strain at failure should be accurately determined. The failure strain is calculated by dividing the ultimate width of crack (which is considered to be equal to half of the fibre length (l_f)) by the characteristic length. It was shown in a previous study on SFRC [45] that using a characteristic length of $h_{sp}/2$ (the depth of a notched prism divided by 2) gives good results when converting displacements into equivalent strains. Thus, for this study, a value of 0.5 was adopted as a strain failure which is fairly close to $l_f/2$ divided by half of the prism depth. It should be noted though that most tests were stopped at 5 mm deflection as not to damage the LVDTs and thus, complete failure was never reached. For design purposes, a max strain of 0.025 is deemed sufficient so as to prevent the development of large crack widths.

The predicted curves are shown together with the experimental results in Figure 16 through Figure 16. As expected, the predictions match well the results.

The results for FCSA at 28 days was further analysed (using the same material model for the 10mm mesh size) with two mesh sizes; 16.6 mm and 5 mm to examine the effect of mesh size. The results (Figure 17) confirm that there is a slight mesh dependence when using this approach.

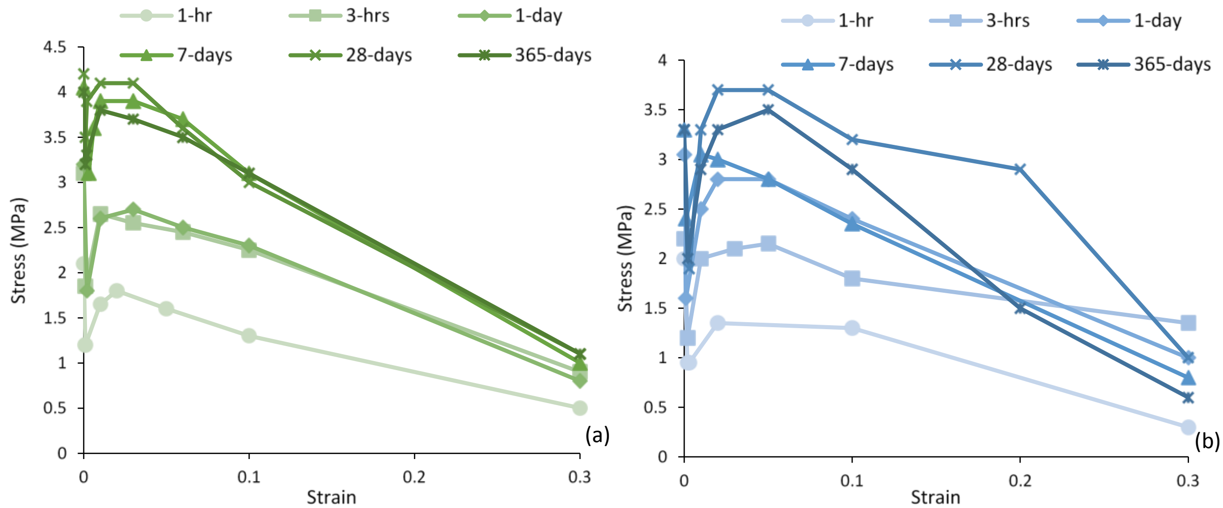

Figure 15. Tensile σ – ε curves for mixes at different ages for: (a) FCSA; (b) FRSC

4.4. Cracking

In the CDP model, cracking can be assumed to initiate at points where the tensile equivalent plastic strain is greater than zero and the maximum principal plastic strain is positive. The direction of the vector normal to the crack plane is assumed to be parallel to the direction of the maximum principal plastic strain [44]. Figure 18 shows maximum principal strain contours for FCSA prism at 28 days. It is clear that the failure of the prisms is characterised by tensile cracking at the midspan of the beam as occurred in the experiments.

The crack width at the bottom of the specimens can be determined from the analysis by examining the spreading of the beam using the horizontal deformation (U_3) as shown in Figure 19. The crack width determined at 3 mm of deflection are compared with CMOD values measured by the clip gauge in Table 4. The predicted values are slightly lower than the experimental values with the biggest error of 14.66% (presented in brackets) for FCSA at 28 days. This confirms that the numerical models were not only successful in predicting the flexural capacity, but also the crack widths of the tested prisms and as a result, they could be used for further studies on repair layers.

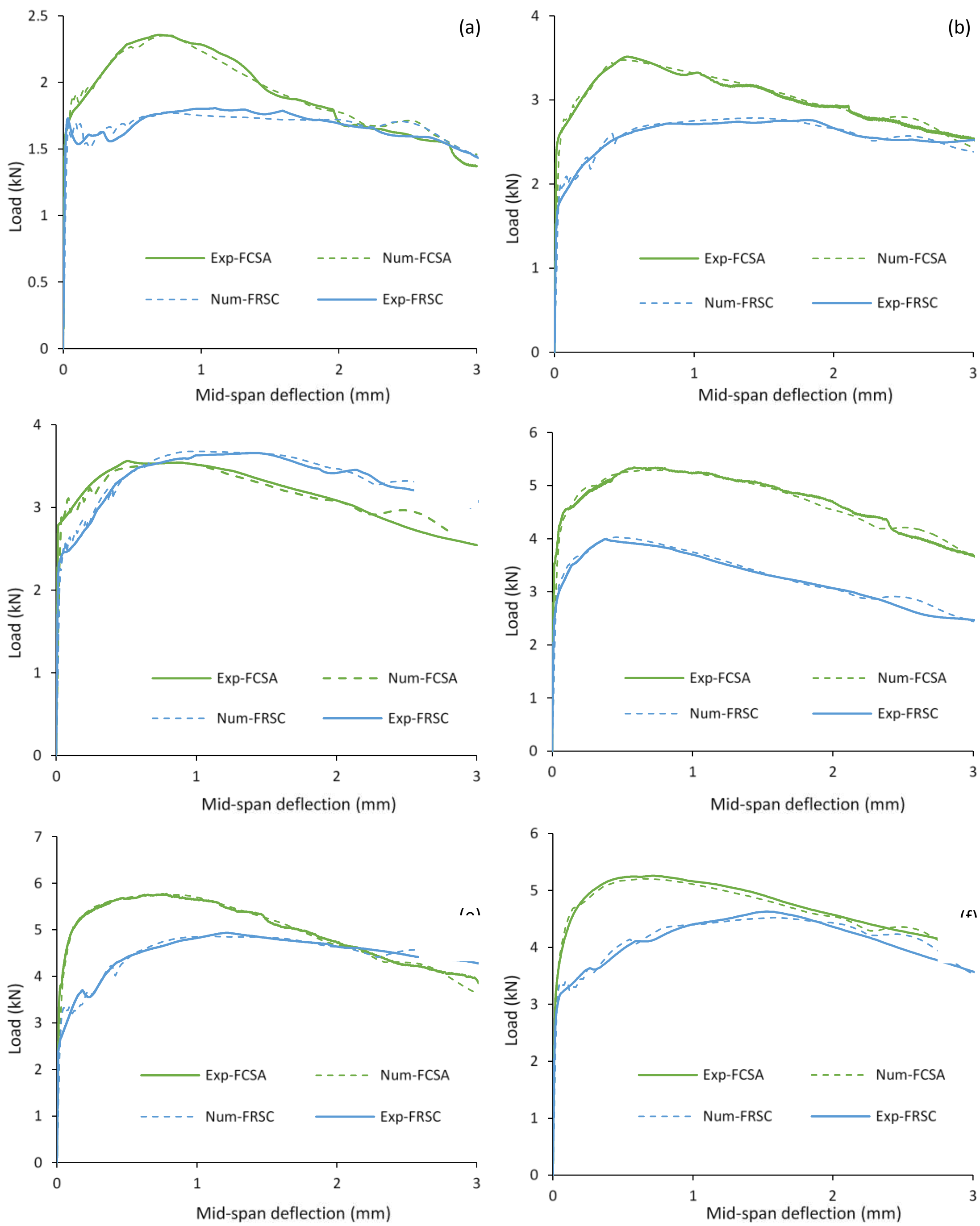

Figure 16. Experimental load-deflection versus numerical curves of FCSA and FRSC prisms at age of: (a) one-hour; (b) three hours; (c) one-day; (d) seven days; (e) 28 days; (f) 365 days

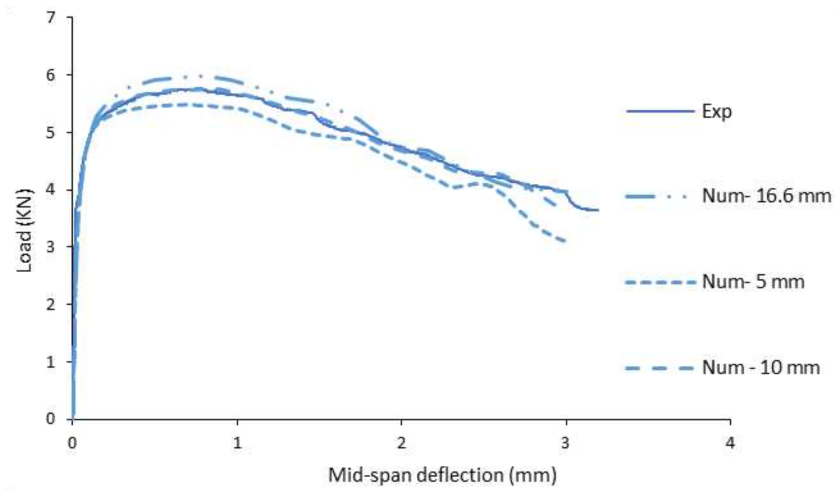

Figure 17. Experimental load-deflection curve of FCSA at 28 days versus numerical curves using three different mesh sizes

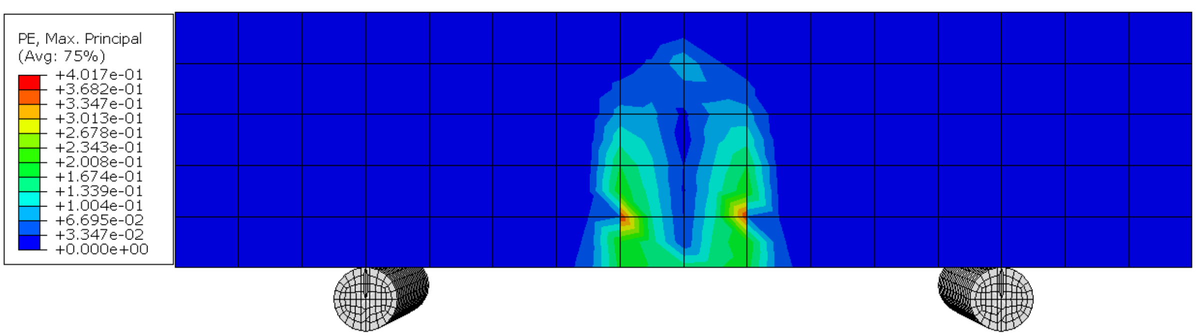

Figure 18. Max principal strain contour for FCSA prisms at 28 days at the end of analysis

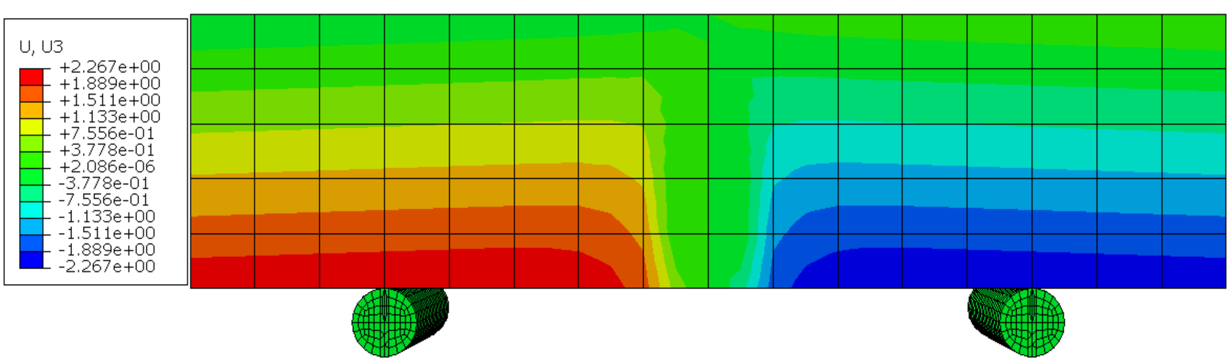

Figure 19. Horizontal displacement (U_3) contour for FCSA prisms at 28 days at the end of analysis

Table 4

The measured and predicted crack widths for fibre reinforced mixes

Mix	Age	1hour	3 hours	1 day	7 days	28 days	365 days
FCSA	Numerical	4.68 (4.10)	4.64 (5.60)	4.68 (5.45)	4.52 (8.87)	4.54 (14.66)	4.64 (9.02)
	Experimental	4.88	4.903	4.953	4.96	5.32	5.10
FRSC	Numerical	4.37 (12.07)	4.60 (8.18)	4.59 (9.82)	4.71 (9.25)	4.57 (12.45)	4.6 (13.21)
	Experimental	4.97	5.01	5.09	5.19	5.22	5.3

Note: Values in brackets represent the error (%) between experimental and numerical crack width

5. Conclusions

Experimental and numerical investigations were performed on plain and fibre reinforced rapid hardening mortars. The main findings of this study are:

- Flexural strength evolves rapidly and both plain and fibre reinforced specimens achieved 90% of their one-year strength in one day. The specimens made with CSA cement showed higher flexural strength than those made with RSC cement tested at the same age due to the rigid dense crystal microstructure of the CSA cement.

- The fibres have a remarkable effect on the strength and modulus of elasticity of prisms. FCSA and FRSC mixes showed a flexural strength increase of approximately 36% to 70% and 24% to 41% respectively. For E_{fm}, an increase of 29.7% was found for FCSA at the age of one-hour. For compressive strength, the highest strength increase of around 24% was observed at one hour. No compressive strength reduction was noticed for any of the mixes tested in this study up to the age of one-year.

- The flexural residual strength for both FCSA and FRSC specimens continued to increase up to 0.7 mm, which corresponds to $CMOD_4$. FCSA prisms show higher f_R than FRSC prisms for the same crack width. The values of f_R continue to increase with time for both FRC mixes and reach their peak values at 28 days. However, there is a slight strength reduction at one year compared to 28 days.
- Strong correlations exist between f_{R1} and f_{R2}, f_{R1} and f_{R3}, f_{R1} and f_{R4} with $R^2 \geq 0.98$ and $R^2 \geq 0.92$ for FCSA and FRSC, respectively.
- FE-predictions using CDP overestimate the loading capacity of FCSA and FRSC when using the tensile constitutive laws based on RILEM TC 162-TDF, CEB FIB MODEL CODE 2010, Barros et al. Conversely, the use of the models proposed by Hu et al. leads to underestimation.
- Inverse analysis was used successfully to obtain multilinear σ – ε tensile curves and model the global load-displacement behaviour.
- Numerical analyses using the refined σ – ε curves were successful in capturing the cracking widths of FRC tested prisms.

Acknowledgments

The authors acknowledge the financial support of the Higher Committee for Education Development in Iraq (HCED-Iraq) for the PhD studies of Hajir Al-musawi. The authors also thank Twincon Ltd for material supply and in-kind contributions.

References

[1] Winnefeld, F., Lothenbach, B., (2010). Hydration of calcium sulfoaluminate cements – experimental findings and thermodynamic modeling. *Cem. Concr. Res*., 40(8), 1239–1247.

[2] Ioannou, S., Paine, K., Quillin, K., (2010). Strength and durability of calcium sulfoaluminate based concretes. In International Conference on Non-Conventional Materials and Technologies: Ecological

Materials and Technologies for Sustainable Building. University of Bath.

[3] Scrivener, K., (2003). Calcium Aluminate Cement. In J. Newman, Advanced Concrete Technology. 2/1-2/29. Oxford: ButterworthHeinemann.

[4] Campas, A., Scrivener, K. (1998). Calcium Aluminate Cements. In A. Campas, & K. Scrivener, Lea's Chemistry of Cement and Concrete, 709-771. Wobum: ButterworthHeinemann.

[5] Banthia, N., Gupta, R., (2009). Plastic shrinkage cracking in cementitious repairs and overlays. *Mater. Struct.*, 42(5), 567–579.

[6] Beushausen, H., Alexander, M.G., (2006). Failure mechanisms and tensile relaxation of bonded concrete overlays subjected to differential shrinkage. *Cem. Concr. Res.*, 36 (10), 1908-1914. Available at: https://www.sciencedirect.com/science/article/pii/S0008884606001608.

[7] Beushausen, H., Chilwesa, M., (2013). Assessment and prediction of drying shrinkage cracking in bonded mortar overlays. *Cem. Concr. Res.*, 53, 256–266. Available at: http://dx.doi.org/10.1016/j.cemconres.2013.07.008.

[8] Banthia, N., Zanotti, C. and Sappakittipakorn, M., (2014). Sustainable fibre reinforced concrete for repair applications. *Constr. Build. Mater.*, 67 (PART C), 405–412. Available at: http://dx.doi.org/10.1016/j.conbuildmat.2013.12.073.

[9] Jewell, R., (2015). Influence of Calcium Sulfoaluminate Cement on the Pullout Performance of Reinforcing Fibres: An Evaluation of the Micro-Mechanical Behavior. PhD Thesis. University of Kentucky. Available at: http://uknowledge.uky.edu/ce_etds/27. [Accessed March 28, 2018].

[10] Swamy, R.N., Stavrides, H., (1979). Influence of fiber reinforcement on restrained shrinkage and cracking. In *Journal Proceedings*. *ACI J.*, 76(3), 443-460.

[11] Graeff, A.G., Pilakoutas, K., Neocleous, K., Peres, M.V.N.N., (2012). Fatigue resistance and cracking mechanism of concrete pavements reinforced with recycled steel fibres recovered from post-consumer tyres. *Eng. Struct.*, 45, 385–395. https://doi.org/10.1016/j.engstruct.2012.06.030.

[12] Pilakoutas, K., Guadagnini, M., (2013). Re-use of steel cord from tyres as reinforcement in sustainable construction – TSB Proposal. The University of Sheffield, Sheffield.

[13] Hu, H., Papastergiou, P., Angelakopoulos, H., Guadagnini, M., Pilakoutas, K., (2018). Mechanical properties of SFRC using blended recycled tyre steel cords and recycled tyre steel fibres, *Constr. Build. Mater*., 187, 553-564.

[14] Frantzis, P., Baggott, R., (2000). Bond between reinforcing steel fibers and magnesium phosphate/calcium aluminate binders. *Cem. Concr. Compos*., 22, 187–192.

[15] Frantzis, P., Baggott, R., (2003). Transition points in steel fiber pullout tests from magnesium phosphate and accelerated calcium aluminate binders. *Cem. Concr. Compos.*, 25, 11–17.

[16] Frantzis, P., (2006). Effect of Early-Age Temperature Rise on the Stability of Rapid-Hardening Cement Fibre Composites. *J. Mater. Civil Eng*., 18, 568–575.

[17] RILEM TC 162-TDF, (2003). σ-ε-design method, *Mater. Struct*., 36(8), 560–567. https://doi.org/10.1007/BF02480834.

[18] F.I. du Béton, (2013). Fib Model Code for Concrete Structures 2010, Wilhelm Ernst & Sohn, Berlin, Germany.

[19] Barros, J.A.O., Cunha, V.M.C.F., Ribeiro, A.F., Antune J.A.B., (2005). PostCracking Behaviour of Steel Fibre-Reinforced Concrete. *Mater. Struct*., 38, 47-56.

[20] Hu, H., Wang, Z., Figueiredo, F., Papastergiou, P., Guadagnini, M., Pilakoutas, K., (2018). Post-

cracking tensile behaviour of blended steel fibre reinforced concrete. *Struct. Concr*. Submitted for publication.

[21] Neocleous, K., Tlemat, H., Pilakoutas, K., (2006). Design issues for concrete reinforced with steel fibers, including fibers recovered from used tires. *J. Mater. Civ. Eng.*, 18(5), 677–685. https://doi.org/10.1061/(ASCE)0899-1561(2006).

[22] Georgin, J.F., Ambroise, J., Péra, J., Reynouard, J.M., (2008). Development of self-leveling screed based on calcium sulfoaluminate cement: Modelling of curling due to drying. *Cem. Concr. Compos*., 30(9), 769-778.

[23] ASTM C191, (2013). Standard Test Method for Time of Setting of Hydraulic Cement by Vicat Needle. *ASTM International*, (May), 1-8.

[24] RILEM, T.C., 119-TCE, (1997). Avoidance of thermal cracking in concrete at early ages. *Mater. Struct*., 30 (202), 451-464.

[25] BS EN 13892-2, (2002). Methods of test for screed materials — Part 2: Determination of flexural and compressive strength.

[26] JSCE-SF4, (1984). Standard for Flexural Strength and Flexural Toughness, Method of Tests for Steel Fiber Reinforced Concrete, Concrete library of JSCE, Japan Concrete Institute (JCI), Japan.

[27] Cost, T., (2008). Practical Semi-Adiabatic Calorimetry for Concrete Mixture Evaluation. In *TTCC/NCC Conference*.

[28] Aiello, M.A., Leuzzi, F., Centonze, G., Maffezzoli, A., (2009). Use of steel fibres recovered from waste tyres as reinforcement in concrete: pull-out behaviour, compressive and flexural strength, *Waste Manage.*, 29, 1960–1970. https://doi.org/10.1016/j.wasman.2008.12.002.

[29] Centonze, G., Leone, M., Aiello, M.A., (2012). Steel fibers from waste tires as reinforcement in concrete: a mechanical characterization. *Constr. Build. Mater.*, 36, 46–57. https://doi.org/10.1016/j.conbuildmat.2012.04.088.

[30] Younis, K.H., Pilakoutas, K., (2013). Strength prediction model and methods for improving recycled aggregate concrete. *Constr. Build. Mater.*, 49, 688–701, https://doi.org/10.1016/j.conbuildmat.2013.09.003.

[31] Bjegovic, D., Baricevic, A., Lakusic, S., Damjanovic, D., Duvnjak, I., (2013). Positive interaction of industrial and recycled steel fibres in fibre reinforced concrete, *J. Civ. Eng. Manage.*, 19, S50–S60. https://doi.org/10.3846/13923730.2013.802710.

[32] Martinelli, E., Caggiano, A., Xargay, H., (2015). An experimental study on the postcracking behaviour of hybrid industrial/recycled steel fibre-reinforced concrete. *Constr. Build. Mater.*, 94, 290–298. https://doi.org/10.1016/j.conbuildmat.2015.07.007.

[33] Hu, H., Papastergiou, P., Angelakopoulos, H., Guadagnini, M. and Pilakoutas, K., (2018). Mechanical properties of SFRC using blended manufactured and recycled tyre steel fibres. *Constr. Build. Mater.*, 163, 376-389. Available at: https://www.sciencedirect.com/science/article/pii/S0950061817325230.

[34] Herrmann, P., (2014). Investigation of fresh and hardened properties of Calcium sulfoaluminate (CSA) cement blends. *Mag. Civ. Eng.*, (3), 63-70. Available at: http://www.engstroy.spb.ru/index_2014_03/07.pdf.

[35] BS EN 14651, (2005). Test method for metallic fibre concrete – Measuring the flexural tensile strength (limit of proportionality (LOP), residual). British Standards Institution, London, UK.

[36] Bordelon, A., (2011). *Flowable fibrous concrete for thin pavement inlays*. PhD Thesis. University of Illinois at Urbana-Champaign.

[37] Younis, K.H., (2014). *Restrained Shrinkage Behaviour of Concrete with Recycled Materials*. PhD Thesis. University of Sheffield.

[38] Jafarifar, N., (2012). *Shrinkage behaviour of steel fibre reinforced concrete pavements*. PhD Thesis. University of Sheffield.

[39] Dawood, E.T., Ramli, M., (2011). High strength characteristics of cement mortar reinforced with hybrid fibres. *Constr. Build. Mater*., 25 (5), 2240-2247.

[40] American Concrete Institute (ACI), (2011). Building code requirements for structural concrete and commentary. (ACI 318M-11) Farmington Hills, MI.

[41] Kosaka, Y., Takeshi, T., Ota, F., (1975). Effect of coarse aggregate on fracture behavior of concrete (part1). *J.A.C.*, 228, 1-11. Cited in Che, Y., (2010). *The development and behaviour of premix GRC suitable for mass produced structural elements*. PhD Thesis, Department of Civil and Structural Engineering, The University of Sheffield.

[42] RILEM. (2002). RILEM TC 162-TDF: Test and design methods for steel fibre reinforced concrete - Bending test, final recommendation. *Mater. Struct.*, 35(253), 579–582.

[43] Zamanzadeh, Z., Lourenço, L. and Barros, J., (2015). Recycled steel fibre reinforced concrete failing in bending and in shear. *Constr. Build. Mater.*, 85, 195–207. Available at: https://doi.org/10.1016/j.conbuildmat.2015.03.070.

[44] ABAQUS 2017 Documentation, [Online].

[45] Tlemat, H., (2004). *Steel fibres from waste tyres to concrete; testing, modelling and design*. PhD Thesis, Department of Civil and Structural Engineering, The University of Sheffield.

[46] Mohsin, S.M.S., (2012). *Behaviour of fibre-reinforced concrete structures under seismic loading*. PhD Thesis. Imperial College London.